

Dhruv Singh
School of Mechanical Engineering and Birck
Nanotechnology Center,
Purdue University,
West Lafayette, IN 47907
e-mail: singh36@purdue.edu

Jayathi Y. Murthy¹
Professor
e-mail: jmurthy@ecn.purdue.edu

Timothy S. Fisher²
Professor
e-mail: tsfisher@ecn.purdue.edu

School of Mechanical Engineering,
Purdue University,
West Lafayette, IN 47907

Phonon Transport Across Mesoscopic Constrictions

Phonon transport across constrictions formed by a nanowire or a nanoparticle on a substrate is studied by a numerical solution of the gray Boltzmann transport equation (BTE) resolving the effects of two length scales that govern problems of practical importance. Predictions of total thermal resistance for wire/substrate and particle/substrate combinations are made for the entire range of Knudsen number, with an emphasis on resolving transport in the mesoscopic regime where ballistic-diffusive mechanisms operate and analytical expressions are not available. The relative magnitudes of bulk and constriction resistance are established, and a correlation for overall thermal resistance spanning the range of practical Knudsen numbers is provided.

[DOI: 10.1115/1.4002842]

Keywords: Boltzmann transport equation, constriction resistance, ballistic-diffusive transition, gas gap conductance, slip flow and heat transfer, Knudsen number, temperature jump

1 Introduction

Thermal contact resistance caused by constrictions or imperfect contacts has long been studied in classical macroscale heat transfer applications such as heat exchangers, fins, composites, and others. With the emergence of new nanomaterials, nanostructures such as nanotubes, nanowires, nanobelts, and nanoparticles have found widespread use in microelectronics, thermal interface materials, thermoelectrics, and other emerging applications [1]. These developments have renewed interest in understanding interface problems that often govern functional performance. Nanoparticles, nanowires, and nanotubes are frequently used in composites, where the overall effective thermal conductivity and behavior at the percolation threshold is limited by the interface resistance [1–4]. In emerging carbon nanotube (CNT) and Si/Ge nanowire field effect transistors (FETs), contact resistance between the device and the substrate on which it lies can dominate the heat flow path [5–7]. For example, the breakdown of single-wall CNTs between metallic contacts is governed by the electrical and thermal contact resistance with the insulating substrates and metallic electrodes rather than the thermal properties of the insulating substrate itself [7,8].

When the nanostructures themselves are highly conducting, the interface forms the critical bottleneck to transport, and a thorough understanding of thermal transport at interfaces is therefore critical. This problem also manifests itself strongly when making practical use of such one-dimensional high thermal conductivity materials [9]. In the engineering of CNT-based thermal interface materials, for example, the interfacial resistance between individual freestanding CNT tips and that between the CNT tip and the substrate on which it is grown can overwhelm the intrinsic thermal resistivity, decreasing the effective or apparent thermal conductivity by as much as two orders of magnitude [10,11]. Particle-filled thermal interface materials often rely on pathways that should exponentially increase the thermal conductivity of such materials above the percolation threshold [12]. However, as length scales decrease, contact resistance begins to dominate the

overall transport such that the apparent thermal conductivity can be less than the host matrix, such as observed with carbon nanotube suspensions [2]. Quantitative prediction of interfacial heat transfer is also essential to the use of thermal scanning probe methods that employ localized heat transfer through the tip of an atomic force microscope (AFM) cantilever, as the accuracy of the temperature map depends intimately on the thermal resistance model used for calibration [13,14].

A number of studies have sought to quantify the thermal resistance of nanowires in contact with substrates [15,16] in geometries similar to that in Fig. 1. Understanding cross-plane phonon transport in this geometry is critical in modeling thermal conductivity and electrothermal transport in Si/Ge nanowire FETs [6], Si nanowire based thin film transistors [17], and thermo-elastic damping in Si nanowire resonators [18]. A similar interest exists in modeling nanoparticle interfaces for applications ranging from aerogels [19,20] and other low thermal conductivity materials [21] to thermal management of metal hydride particle beds [22]. Here, a nanowire or a nanoparticle is situated between substrates under an imposed temperature difference ($T_1 - T_2$). The overall thermal resistance is the sum of the resistances offered by the substrates, constrictions, and the wire or particle. Previous research has approximated this overall resistance with the constriction resistance, either using the ballistic limit value R_{cb} or an approximation based on the sum of the diffuse and ballistic constriction resistances R_{cd} and R_{cb} [15,23–25]. These expressions have been developed for point contacts to infinitely large objects. However, current applications such as wires and particles in contact have two defining length scales: the diameter of the wire/particle (D), and the contact width/radius (a). A strict definition of a transition regime under such conditions is difficult to establish. For example, there may be enough bulk phonon-phonon scattering that phonon transport in the bulk of the particle is diffusive, even though the contact length scale is still on the order of phonon mean free path l or smaller. The neglect of wire and particle resistance is valid only in the limit of high particle conductance. This circumstance occurs for extremely small constrictions or at very low temperatures. Furthermore, in the transition regime between the ballistic and diffuse limits, the overall thermal resistance is not a simple addition of the ballistic and diffusive components. Therefore, the objective of this paper is to identify and quantify the ballistic-diffusive transition in thermal resistance across these contacts as a function of the wire/particle Knudsen number.

¹Corresponding author.

²Present address: Air Force Research Laboratory Thermal Sciences and Materials Branch (AFRL/RXBT), Wright-Patterson AFB, OH 45433-7750.

Contributed by the Heat Transfer Division of ASME for publication in the JOURNAL OF HEAT TRANSFER. Manuscript received December 21, 2009; final manuscript received June 29, 2010; published online January 11, 2011. Assoc. Editor: Andrey Kuznetsov.

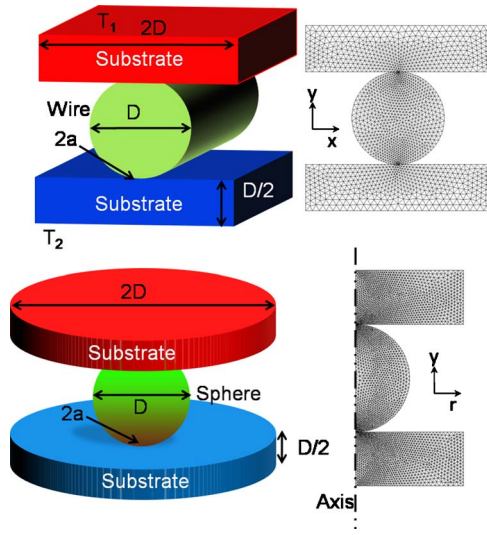


Fig. 1 Schematic of the geometry being simulated and the corresponding computational mesh. The contact width of the nanowire with the substrates is $2a$ and D is the wire diameter (top). The contact diameter of a nanoparticle with substrates is $2a$ and D is the particle diameter (bottom). A 2D axisymmetric model of particle on substrate is simulated.

When the contact radius a is much less than the phonon mean free path l , the thermal constriction resistance in the ballistic limit R_{cb} is given as [15,23,25]

$$R_{cb} = \frac{4}{Cv_g A} = \frac{4}{3\pi k a} \text{Kn} \quad (1)$$

where $A = \pi a^2$ is the contact area, k the bulk thermal conductivity of the wire and substrate, and $\text{Kn} (=l/a)$ is the Knudsen number of the contact. In the diffusive limit, the constriction resistance R_{cd} depends on the geometry of the constriction and bulk contact but varies inversely as the shape factor $2a/D$, where D is the diameter of the particle or wire. Analytical expressions for the thermal constriction resistance as calculated by a solution of the diffusion equation may be found in Ref. [26] for cylinder and in Ref. [27] for a sphere between two plates. In the transition regime ($a \sim l$), phonon bulk scattering begins to play a role, and a direct solution of the phonon Boltzmann transport equation must be used in order to predict the heat flux crossing the constriction. Analytical solutions have been obtained by Wexler [23] and Nikolic and Allen [25] for a point contact between two infinite reservoirs for a range of Kn . A similar analysis for the ballistic-diffusive transition of thermal resistance for a wire in the axial direction is presented in Ref. [28]. Analytical solutions of the Boltzmann transport equation for in-plane conductivity of thin films and axial conductivity of wires exists for a range of Kn [29]. An empirical estimate of the resistance in the intermediate Kn regime has generally been expressed in the form

$$R_c(\text{Kn}) = R_{cb} + \gamma(\text{Kn})R_{cd} \quad (2)$$

where R_{cb} is calculated using Eq. (1) and $R_{cd} = 1/(2ka)$ for a circular contact between two infinite reservoirs. Values of γ were obtained in Ref. [23] in the mesoscopic regime and reported to range from 0.6 to 1.0 for a circular contact. Because $R_{cd} \sim 1/a$ and $R_{cb} \sim l/a^2 \sim \text{Kn}/a$, the interpolation in Eq. (2) works well in the limits $\text{Kn} \rightarrow 0$ and $\text{Kn} \rightarrow \infty$. For the transition regime, γ depends on the specific geometry under consideration. Furthermore, the contact width $2a/D$ is of order 0.01 to 0.1 for practical circumstances [16]. Because $l/D \rightarrow a/D$ as $l/a \rightarrow 1$, the thermal resistance within the wire/particle may become a significant contribu-

tor for mesoscale constrictions and may compete with the constriction resistance.

In this paper, we employ a numerical solution of the gray phonon Boltzmann transport equation to compute thermal resistance for the arrangements shown in Fig. 1 over a range of wire/particle Knudsen numbers. We identify the contributions of the different resistance components and quantify the error engendered in simple additive resistance approximations. In formulating the Boltzmann transport equation, we assume an incoherent particle model of phonon transport with the group velocity and scattering rate of bulk silicon. In doing so, we also ignore the possibility of reduction in phonon transmission due to a mismatch in phonon dispersion of the particle/wire and substrate (bulk Si). Recent work indicates that such mismatch will be significant only for nanowires of diameter below 10 nm at room temperature [30]. Wave effects become the dominant mechanism in impeding thermal transport across contacts at low temperatures (the wavelength of the dominant phonons in Si at 1 K is ~ 100 nm). This was demonstrated in the experiments performed by Schwab et al. [31] who measured the quantum of thermal conductance using a nanomembrane attached to heaters through a contoured bridge. Theoretical studies [32,33] and nonequilibrium molecular dynamics simulations [34] in silicon, however, indicate that these effects are limited to low temperatures. At room temperature, the dominant phonon wavelength is small enough that constrictions larger than 1 nm do not exhibit reduced thermal conductance due to wave effects and surface reconstruction does not affect phonon transmission [34]. The assumption of a monolithic contact in the current study discounts reduced phonon transmission that may occur due to noncovalent van der Waals (VW) interactions between the two bodies. The present study of monolithic contacts render mode-dependent phonon effects negligible because of the matched phonon dispersion. This situation is in contrast to the study of heterojunctions such as those in a superlattice (where spectral mismatch plays a significant role) or of electron-phonon coupling in MOSFETs for which phonon emission is favored in a particular frequency range. Similar gray Boltzmann transport equation (BTE) computations have also been employed by Chung and Kaviani [35] for modeling effective thermal conductivity of porous silicon over a wide size range.

Details of the computational model and numerical implementation of the BTE are given in Sec. 2. Section 3 presents results for thermal resistance based on a gray approximation of the BTE. Section 4 includes a brief discussion of alternative thermal pathways between the two substrates—namely, conduction through the surrounding gas gap and radiation between the two substrates.

2 Computational Model

The 2D geometry shown in Fig. 1 involves a nanowire or spherical nanoparticle located between two substrates of the same material, forming a nanoscale line contact (in the case of a wire) or a circular contact (in the case of a sphere) at the interface. The width of the contact, $2a$, is computed nominally as in Ref. [31]. The wire and particle are assumed perfectly circular. Under the assumptions outlined in the previous section, phonon transport in the wire and substrate may be described by the BTE.

2.1 Gray Approximation. The Boltzmann transport equation for the energy density of phonons under a gray assumption [36] within the relaxation time approximation may be expressed as

$$\nabla \cdot (v_g s e'') = \frac{e^0 - e''}{\tau} \quad (3)$$

Here, $e''(\mathbf{r}, s)$ is the net energy density ($\text{J}/\text{m}^3 \text{sr}$) of all phonon groups at position \mathbf{r} and in direction s . The quantity $e^0(\mathbf{r})$ represents the angular average of $e''(\mathbf{r}, s)$ over all directions s at a given position \mathbf{r} .

$$e'' = \sum_p \left(\int f \hbar \omega D_p(\omega) d\omega \right) e^0 = \frac{1}{4\pi} \sum_p \left(\int_{4\pi} e'' d\Omega \right) \quad (4)$$

Here, f is the nonequilibrium distribution function of the phonons, ω is their angular frequency, p is the phonon polarization, $D_p(\omega)$ is the density of phonon states, and $d\Omega$ is the incremental solid angle. The gray BTE treats phonons of all polarizations and wavevectors as having the same group velocity v_g and a single relaxation time τ . The group velocity v_g is chosen to reflect the velocity of the dominant phonon groups at the temperature under consideration, and τ is chosen so as to recover Fourier's law at $\text{Kn} \ll 1$ with a thermal conductivity, $k = Cv_g^2\tau/3$, at the required temperature, where C is the volumetric specific heat capacity of the solid. The temperature field is obtained as

$$T(\mathbf{r}) = \frac{1}{4\pi C} \int_{4\pi} e''(\mathbf{r}, \mathbf{s}) d\Omega \quad (5)$$

2.2 Boundary Conditions

2.2.1 Fixed-Temperature Boundaries. For a boundary with given temperature $T=T_b$, the energy density of all wavevector directions entering the domain from the boundary ($\mathbf{s} \cdot \mathbf{n} \leq 0$) is given by

$$e'' = e^0 = \frac{CT_b}{4\pi} \quad (6)$$

Here, \mathbf{n} is the outward-pointing normal from the domain. The volumetric specific heat C is assumed to be constant because the temperature difference ($T_1 - T_2$) is small. For all directions pointing toward the boundary from the interior of the domain, the following boundary condition is used.

$$\nabla e'' \cdot \mathbf{s} = 0 \quad (7)$$

2.2.2 Diffusely Reflecting Boundaries. The interface value of e'' at a diffusely reflecting interface for all directions incoming to the domain ($\mathbf{s} \cdot \mathbf{n} \leq 0$) is given by

$$e''(\mathbf{r}, \mathbf{s}) = \frac{1}{\pi} \int_{\mathbf{s} \cdot \mathbf{n} > 0} e'' \mathbf{s} \cdot \mathbf{n} d\Omega \quad (8)$$

The wire/particle and substrate walls are assumed to reflect diffusely because the wavelength of dominant phonon groups near room temperature is less than the typical surface roughness scale.

2.2.3 Symmetry Boundaries. Phonons are assumed to reflect specularly at all symmetry boundaries on the substrate. For all directions incoming to the substrate ($\mathbf{s} \cdot \mathbf{n} \leq 0$),

$$e''(\mathbf{s}, \mathbf{r}) = e''(\mathbf{s}_r, \mathbf{r}) \quad (9)$$

where \mathbf{s}_r is the incoming specular direction corresponding to \mathbf{s} :

$$\mathbf{s} = \mathbf{s}_r - (2\mathbf{s}_r \cdot \mathbf{n})\mathbf{n} \quad (10)$$

When gas gap conduction is considered for symmetry boundaries bounding the gas domain, a zero normal temperature gradient condition applies

$$\nabla T \cdot \mathbf{n} = 0 \quad (11)$$

where \mathbf{n} is the unit normal to the symmetry boundary.

Nondimensionalization of the governing equation yields the following dimensionless parameters

$$D^* = \frac{D}{v_g \tau}, \quad 2a^* = \frac{2a}{v_g \tau} \quad (12)$$

where D^* is the acoustic thickness of the wire/particle (inverse Knudsen number) based on its diameter, and $2a^*$ is the aperture thickness (inverse Knudsen number based on the dimension of the contact).

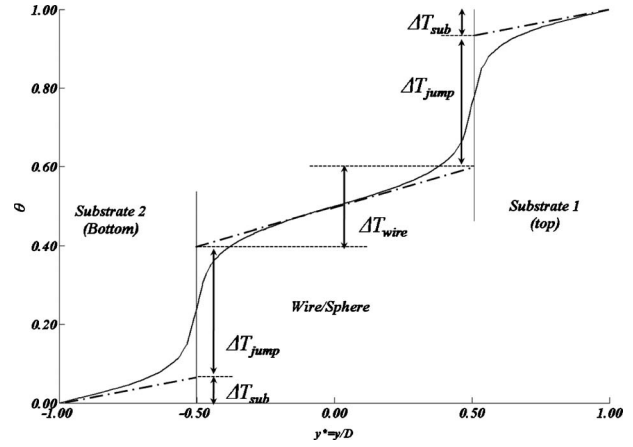


Fig. 2 Definition of ΔT_{jump} , ΔT_{wire} , and ΔT_{sub} : the solid line shows the computed temperature profile and dash-dotted lines show the fitted temperature profile in each section

2.3 Numerical Method. The BTE is solved using a finite volume method described previously [36,37]. Figure 1 shows the unstructured meshes for both the wire and particle cases used in most computations. Mesh independence tests were conducted for a nanowire-substrate case with $D^* = 1.54$ and $2a^* = 0.045$ using meshes of 1294 cells, 5174 cells, and 20,696 cells, and the computed thermal resistance did not change by more than 0.4% between the 5174 cell and the 20,696 cell meshes. Therefore, a 5174 cell mesh was used for most computations presented in this paper, though finer meshes are used at larger acoustic thicknesses. An angular discretization of 4×4 control angles in the octant is used; comparisons with a finer discretization of 12×12 in the octant yielded a difference of less than 0.5% in the constriction resistance. Similar tests were done for the particle-substrate case and an unstructured mesh of 6967 cells as shown in Fig. 1. However as the acoustic thickness increases and becomes larger than 10, a finer discretization is required near the boundaries. Finer meshes are used for cases when $D^* > 10$.

2.4 Estimation of Resistance. The computed bulk temperature profile in the substrates is extrapolated linearly on both sides of the constriction to the interface. The heat transfer rate Q is obtained directly from the simulation. In the bulk of the wire (sphere), the slope of the temperature profile in the central portion is extrapolated to either end of the wire (sphere) to capture the effects of the constriction. Subsequently, the temperature jump across the constriction, ΔT_{jump} is computed as

$$\Delta T_{\text{jump}} = \frac{D}{2} \left(\left. \frac{\partial T_{\text{sub}}}{\partial y} \right|_{y=D} - \left. \frac{\partial T_{\text{wire}}}{\partial y} \right|_{y=0} \right) = \frac{1}{2} \left(\left. \frac{\partial T_{\text{sub}}}{\partial y^*} \right|_{y^*=1} - \left. \frac{\partial T_{\text{wire}}}{\partial y} \right|_{y^*=0} \right) \quad (13)$$

The corresponding temperature drops in the wire/sphere and the substrates due to three-phonon scattering may be calculated similarly and are denoted as ΔT_{wire} , ΔT_{sphere} , and ΔT_{sub} . These are schematically shown in Fig. 2. We define the wire and substrate resistances encountered in the configuration shown in Fig. 1 as $R_{\text{wire}} = \Delta T_{\text{wire}}/Q$; $R_{\text{sub}} = \Delta T_{\text{sub}}/Q$. The total resistance of the complete configuration R_{tot} is given by $Q/(T_1 - T_2)$. The total resistance computed using the Fourier conduction model is denoted by $R_{\text{tot},d}$.

3 Results and Discussions

Computed resistances are presented below in terms of the non-dimensional groups $D^* (=D/v_g \tau)$ and $2a^* (=2a/v_g \tau)$. For a silicon

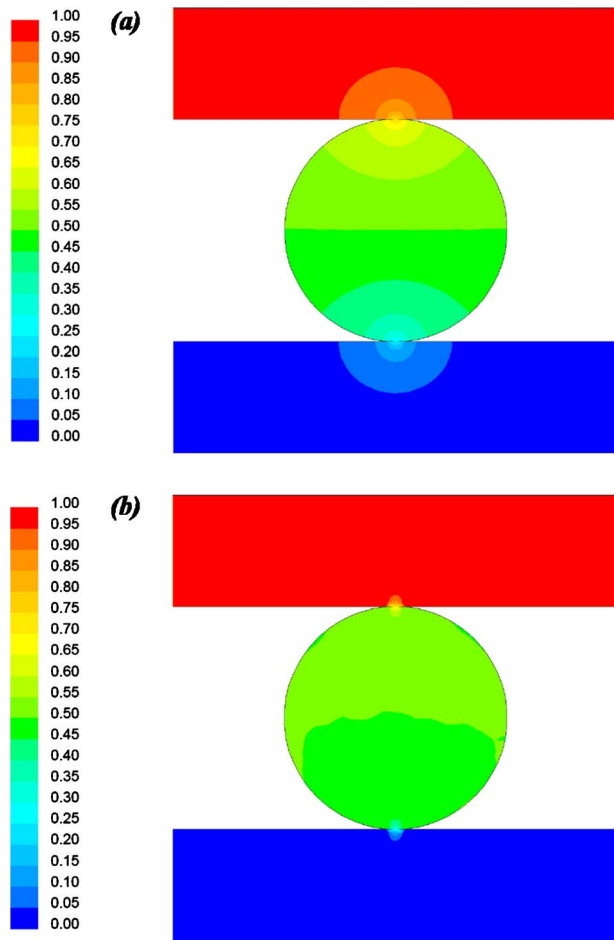


Fig. 3 Contours of dimensionless temperature in wire and substrates for (a) Fourier conduction and (b) gray BTE for $D^* = 0.15$ and $2a^* = 0.45 \times 10^{-2}$

nanowire of diameter $D=40$ nm lying on a silicon substrate, the contact width as estimated using a van der Waals attraction force and Hertzian contact theory [16] is $2a=1.2$ nm. A similar estimate for a sphere of diameter $D=40$ nm gives $2a=1.6$ nm. Furthermore, following the phonon branch averaging procedure of Chen [38], we use $v_g=1804$ ms $^{-1}$, $C=0.93 \times 10^6$ J/m 3 K, and $l=v_g\tau=260.4$ nm to calculate the nominal values of the dimensionless parameters as $D^*=0.15$ and $2a^*=0.45 \times 10^{-2}$. Contours of the dimensionless temperature $\theta=(T-T_2)/(T_1-T_2)$ are plotted in Fig. 3 using the Fourier conduction and gray BTE models. Thermal conductivity is derived from the phonon specific heat, velocity, and scattering rate for the Fourier calculations as $k=Cv_g^2\tau/3$. Figure 4 shows the corresponding dimensionless temperature along the centerline of the wire as predicted by the Fourier and gray BTE models for the nominal case and $2a^*=0.0135$. The BTE results reveal that the substrate temperatures are nearly uniform at $\theta=1$ and $\theta=0$, while the wire temperature is nearly uniform at $\theta=0.5$, commensurate with nearly ballistic transport in both the wire and the constriction. For the 40 nm diameter silicon wire considered here, the contact dimension $2a \approx 0.03D$ ($\approx 0.04D$ for the sphere) dictates that transport in the constriction region is nearly ballistic for sufficiently small D^* . In this limit, the ballistic constriction resistance R_{cb} (see Eq. (1)) is the appropriate resistance to use [14]. In contrast, the temperature field predicted by the Fourier model has a diffusive character, and the contact resistance resulting from the Fourier prediction is significantly smaller than that predicted by the BTE (or than using Eq. (1)).

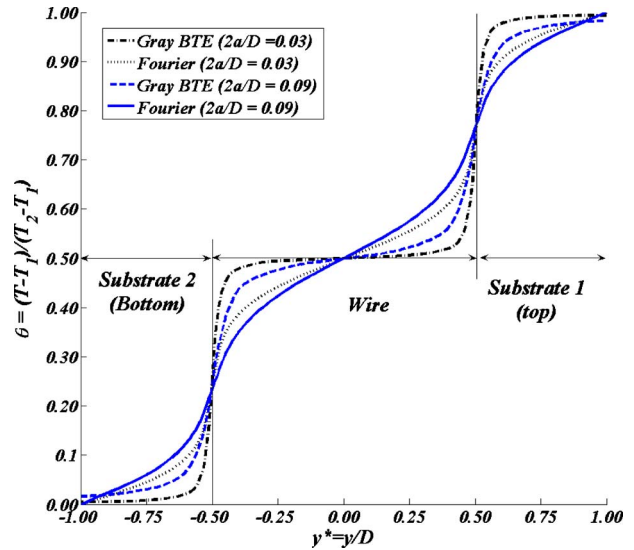


Fig. 4 Temperature distribution along the center line for wire between substrates by Fourier diffusion and gray BTE for $D^* = 0.15$ and $2a/D=0.03, 0.09$

Effect of Wire/Particle Acoustic Thickness. We now consider the effect of acoustic thickness D^* for a fixed value of $2a/D=0.03$. All reported resistances are normalized by R_{cb} (Eq. (1)) and are plotted versus D^* in Fig. 5. For $D^* < 0.1$, the wire and substrate resistances contribute less than 5% of the total resistance computed by the BTE and can be neglected with impunity. As the wire diameter becomes greater than the bulk phonon mean free path, phonon-phonon scattering in the wire increases rapidly; by $D^* \approx 15$ ($2a^* \approx 0.45$), bulk scattering in the wire accounts for as much as 40% of R_{tot} . Assuming a phonon mean free path in silicon of approximately 260 nm at room temperature [38], these results suggest that wire resistance is significant only for wire diameters greater than approximately 1 μ m. For diameters below 260 nm at room temperature, the error engendered by ignoring wire resistance is less than 5% but may become significant for wire constrictions at higher temperatures as the phonon mean free path decreases. The substrate resistance also follows the same

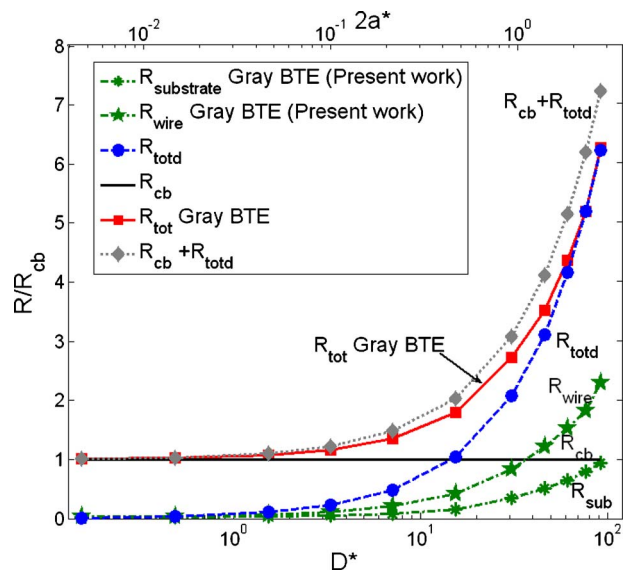


Fig. 5 Variation of contact resistance with D^* for a wire between substrates, $2a/D=0.03$

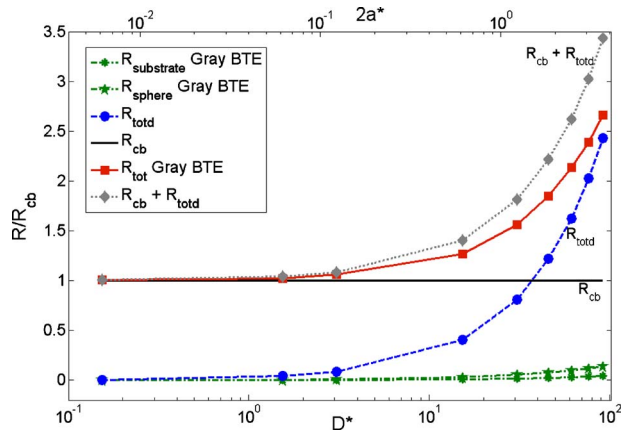


Fig. 6 Variation of contact resistance with D^* for a sphere between substrates, $2a/D=0.04$

trend.

The diffusive resistance $R_{tot,d}$, obtained by the numerical solution of Fourier diffusion equation, severely underpredicts R_{tot} for $D^* < 10$. Likewise, the ballistic resistance R_{cb} is significantly smaller than R_{tot} for $D^* > 10$. Figure 6 shows similar results for the case of a spherical constriction. In the case of a sphere, the constriction is much more abrupt, and hence phonon scattering in the bulk of the particle is negligible even in the diffuse limit. The overall thermal resistance is governed primarily by scattering at the constriction (boundary scattering for $2a^* \ll 1$ and phonon-phonon scattering at $2a^* \gg 1$).

For the range $1 < D^* < 100$ (i.e., $0.03 < 2a^* < 3$) in Fig. 5, the transport in the constriction region becomes increasingly diffusive, and neither the diffusive resistance as calculated from the Fourier diffusion equation nor the ballistic resistance produces satisfactory estimates of the total resistance between the two substrates. It has been suggested [15,23–25] that in this transition regime, an estimate of the constriction resistance can be made by simply adding R_{cb} and R_{cd} or by introducing a correction factor γ as in Eq. (2). Figure 6 shows the variation of the parameter γ in the simple additive formula as a function of the normalized contact spot size $2a^*$. The formula works reasonably well for $2a^* < 0.1$ with $\gamma=0.76$ for a cylinder and $\gamma=0.63$ for a sphere and point contact. As the constriction width increases into the range $0.1 < 2a^* < 10$, significant departures from the simple additive model appear, and in this regime, γ varies with the contact spot size. Then, for $2a^* > 10$, the additive model converges toward a constant γ value of unity. Following [23], we compute a correction factor γ for the two types of constrictions, defined as

$$R_{tot}(a^*) = R_{cb} + \gamma(a^*)R_{tot,d} \quad (14)$$

We find through simple curve fitting that $\gamma=(1+4.97/2a^*)/(1+6.52/2a^*)$ for a wire and $\gamma=(1+7.32/2a^*)/(1+11.66/2a^*)$ for a sphere. These functions are also plotted in Fig. 7 along with the factor $\gamma=(1+0.83/2a^*)/(1+1.33/2a^*)$ for a point contact, computed in Ref. [23]. The value of this correction factor depends on the shape of the constriction for the cases considered here and varies by nearly a factor of 2 in the mesoscopic regime. Values of γ yield the same form in the transition regime for the contact formed by sphere on a substrate and that of a point contact between two infinite spheres because the shape of the two contacts is circular (~ 0.62 as $2a^* \rightarrow 0$). The constriction formed by a wire on a substrate is rectangular and has a slightly different limit as $2a^* \rightarrow 0$.

The effect of varying the contact width ($2a/D$) at a constant wire acoustic thickness D^* has also been investigated. Though an estimation of a may be obtained as in Ref. [16], there is uncertainty in the computed value because of the uncertainties in the

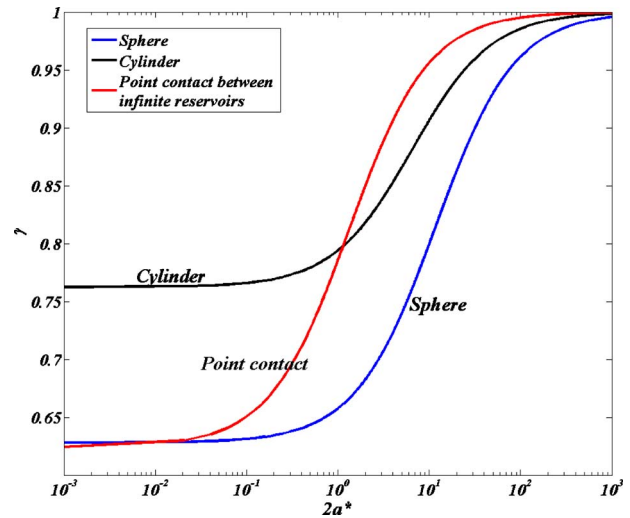


Fig. 7 Correction factor γ as a function of $2a^*$ for wire, sphere, and point contact

force constants and the neglect of self-weight and other forces. Figure 8 shows the variation of the total resistance R_{tot}/R_{cb} for $D^*=0.15$ and 1.5 . Also shown is the relative magnitude of bulk scattering in the wire characterized by R_{wire}/R_{cb} . The computed values are very close to unity at $D^*=0.15$, which is expected because the constriction is ballistic in this range ($2a^* = 0.0045-0.0135$). At $D^*=1.54$ ($2a^*=0.045-0.135$), however, some diffusive effects exist. These effects are not very strong for the range of D^* investigated. Interestingly, as the contact width increases, the bulk scattering in the wire becomes more significant in comparison to constriction resistance even at low D^* and scales almost linearly. As the contact width increases, the bulk scattering in the wire starts to become more significant in comparison to constriction resistance even at low D^* and R_{wire}/R_{cb} scales almost linearly. These simulations indicate that the ballistic limit is attained for both wire and particle between substrates when $D^* \sim 1$, indicating that though there is some phonon-phonon scattering in the bulk of the wire, the constriction resistance far overwhelms this and governs the transition to the ballistic limit. On the other hand, the computations line up with the diffuse prediction by

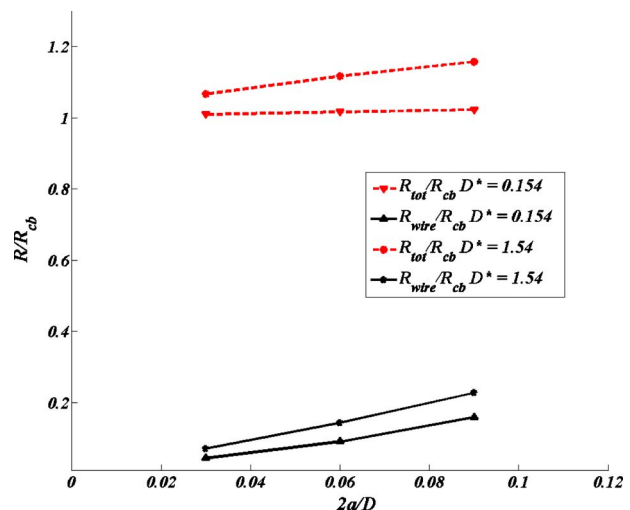


Fig. 8 Variation of constriction resistance with constriction width $2a/D$

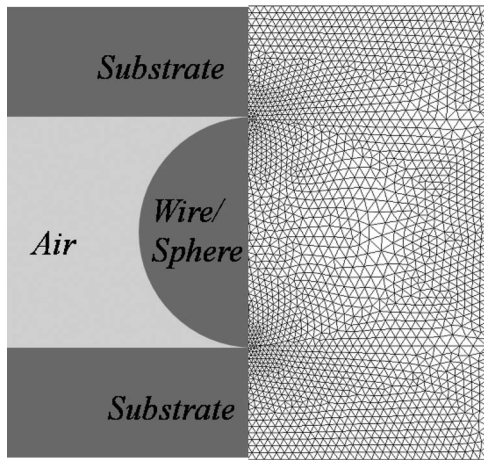


Fig. 9 Schematic of the geometry and unstructured mesh used in coupled BTE-Fourier slip calculation

$2a^* \sim 3$ ($D^* \sim 100$) showing that bulk scattering in the wire (equivalently the wire length scale) indeed determines the transition to the diffuse limit.

4 Effect of Gas Gap Conduction

An assessment of the alternative pathways for heat transfer is also relevant for practical problems. The presence of a conducting gas in the gap between the substrates can act as a complementary pathway for heat transfer. Because air molecules at standard temperature and pressure (STP) have a mean free path of about 65 nm, it is necessary to incorporate a finite temperature jump at the boundaries. To mimic the effects of heat transfer by air molecules in the subcontinuum regime, we solve the diffusion equation for heat conduction in air with temperature slip at the solid boundaries (rather than a full invocation of the Boltzmann kinetic model for gas molecules [39]) in conjunction with the phonon BTE in the solid (Eq. (3)),

$$k_{\text{gas}} \nabla^2 T = 0$$

$$T_{\text{slip}} = T_{\text{wall}} + \frac{2 - \alpha_g}{\alpha_g} \frac{2\eta}{\eta + 1} \frac{2\mu}{\rho} \sqrt{\frac{\pi}{8RT\text{Pr}}} \frac{1}{\rho} \left(\frac{\partial T}{\partial n} \right)_{\text{slip}} \quad (15)$$

where n is the local normal coordinate at the gas-solid interface, α_g is the accommodation coefficient of gas molecules on the solid surface, μ is the viscosity of the gas, η is the ratio of specific heats, and ρ is the gas density. Overall thermal conductance can be calculated to reasonable accuracy even with this approximation [40,41]. For detailed modeling results of thermal transport employing a simultaneous solution of the gas phase and phonon Boltzmann equation, the reader is referred to Ref. [42]. Typical accommodation coefficients for air on oxide-terminated surfaces is $\alpha_g \approx 0.9$, $\eta = 1.4$. The schematic and mesh details of the computational domain are shown in Fig. 9. When gas gap conduction is included, the net phonon energy flux leaving the wire/substrate must balance the Fourier heat flux in the gas. The net phonon energy flux leaving the wire or substrate is the difference of the incoming phonon flux, the reflected phonon flux, and the phonon emission at the interface due to the interface temperature [41]. Assuming diffuse emission and that the emissivity of phonons is equal to the absorptivity ($=1$), the interfacial heat balance can be expressed as

Table 1 Ratio of thermal conductance with and without conducting gas in the gap between the substrates as a function of particle diameter for $2a/D=0.04$. Standard temperature and pressure are assumed. $k_f^* = 1.66 \times 10^{-4}$

Particle diameter (nm)	Ratio of thermal conductance with and without gas	Kn_g
40	1.42	3.39
120	1.37	1.13
240	1.30	0.57
480	1.24	0.28
720	1.20	0.18
1440	1.16	0.094
2880	1.13	0.047

$$-k_f \nabla T_{\text{slip}} \cdot n = \left(\int_{s \cdot n > 0} v_g e'' \cdot s \cdot n d\Omega + \int_{s \cdot n \leq 0} v_g e^0 \cdot s \cdot n d\Omega \right) \quad (16)$$

The nondimensional parameters arising out of this coupling are the ratio of solid to gas thermal conductivities and a Knudsen number based on the temperature slip length of gas molecules,

$$k_f^* = \frac{k_f}{Cv_g^2 \pi / 3}; \quad \text{Kn}_g = \frac{\left(\frac{2 - \alpha_g}{\alpha_g} \frac{2\eta}{\eta + 1} \frac{2\mu}{\rho} \sqrt{\frac{\pi}{8RT\text{Pr}}} \frac{1}{\rho} \right)}{D} \quad (17)$$

The relative contribution of heat conduction through the gas gap to the total thermal conductance increases as the length scale decreases (because the thermal conductance of the solid contact decreases). Simulations including gas gap conduction for the wire indicate an increase in thermal conductance of less than 4% for a wire of diameter 40 nm ($2a = 1.2$ nm). As the length scale increases, the contribution of gas gap conduction decreases. Therefore, most heat conducts through the solid at STP. However, conduction through the gas phase can be competitive with that through the solid at higher gas pressures. An estimate of thermal conductance without interfacial temperature slip indicates that conductance may increase by more than 100% over the value without the gas.

For the sphere, however, the constriction is three-dimensional and has significantly higher resistance (lower conductance) than a two-dimensional constriction as in the case of a wire. Thermal conductance is significantly increased by the presence of a surrounding medium. Simulations reveal that the conductance increased by 40% for a 40 nm particle between substrates ($2a = 1.6$ nm) even when the gas phase is in the high Km regime. As ambient pressure of the gas is increased the gas gap may be the determining pathway for heat transfer. When temperature slip in the gas is not included in the simulations, conductance increases eightfold. Table 1 shows the ratio of thermal conductance with and without the presence of surrounding gas gap for different particle sizes with $2a/D = 1.6$ nm. The contribution of the gas gap to thermal conductance decreases as the constriction becomes less and less resistive and is less than 10% for particle sizes greater than 10 μm . Figure 10 shows the temperature contours including gas gap conduction for particle of size 40 nm (left) and that for 2.8 μm (right). The temperature drop within the gas gap in the high Kn regime is highest across the solid-gas interfaces while for the larger particle, conduction through air is almost diffuse and increases conductance by 13% (Table 1).

Thermal radiation between the two substrates through the gas gap may also play a role in heat transfer. At a temperature of 300 K, the blackbody radiative heat flux is found to be nearly five orders of magnitude smaller than that due to phonon transport. Near-field enhancement for silicon without doping may increase

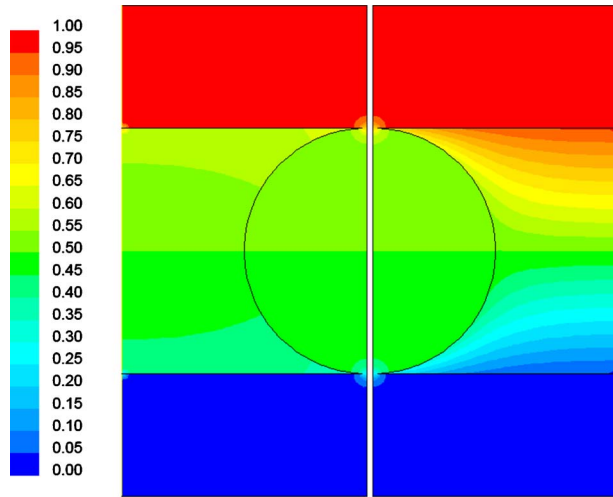


Fig. 10 Contours of nondimensional temperature for thermal conduction across nanoparticle of diameter 40 nm (left) and 2.8 μm (right) sandwiched between two substrates with air in the surrounding gap. $2a/D=0.04$

radiation heat transfer by approximately an order of magnitude as compared with blackbody radiation [43], but the overall effect is still far smaller than the phonon contribution.

5 Conclusions

In this paper, the phonon Boltzmann transport equation is solved for a wire or a particle sandwiched between two substrates to compute the overall thermal resistance in the mesoscopic regime. The ballistic expression for resistance to heat flow ($4/Cv_g A$) is found to be valid for as long as the aperture thickness $2a^* \ll 1$, but departure from this value is seen at lower particle or wire Knudsen numbers. For the transition regime, where bulk scattering effects are not negligible, it is found that the predicted total resistance departs significantly from both the ballistic and diffuse estimates. Curve fits to the computed resistance are provided in the form of a correction factor γ , which shows a dependence on constriction geometry in the mesoscopic regime. The resistance due to the bulk of the wire becomes important only for relatively large-diameter wires in the micron range. For spherical particles, the bulk resistance does not play a role even for very large particles. Gas gap conduction may be the primary pathway for heat transfer between the nanoparticle and substrate or nanoparticles in contact with each other.

Acknowledgment

The support of Air Force Research Laboratory and P.C. Krause & Associates is gratefully acknowledged. J.M. wishes to acknowledge support from Purdue's Network for Computational Nanotechnology, and the use of NANO HUB. See <http://www.nanohub.org>.

Nomenclature

- $2a$ = contact width/diameter (m)
- $2a^*$ = aperture/contact acoustic thickness
- A = contact area (m^2)
- C = volumetric specific heat of phonons ($\text{J m}^{-3} \text{K}^{-1}$)
- D = diameter of the wire/particle (m)
- D^* = wire/particle acoustic thickness
- e'' = directional phonon energy density ($\text{J m}^{-3} \text{sr}^{-1}$)
- e^0 = angular average of directional phonon energy density ($\text{J m}^{-3} \text{sr}^{-1}$)

- \hbar = reduced Planck constant (J-s)
- k = bulk thermal conductivity of solid ($\text{W m}^{-1} \text{K}^{-1}$)
- k_{gas} = thermal conductivity of gas molecules ($\text{W m}^{-1} \text{K}^{-1}$)
- Kn = Knudsen number for the contact
- Kn_g = Knudsen number for gas molecules
- l = phonon mean free path (m)
- \mathbf{n} = unit normal vector to the surface
- Pr = Prandtl number
- \mathbf{r} = position vector (m)
- R = universal gas constant ($\text{J K}^{-1} \text{mol}^{-1}$)
- R_c = constriction resistance (K/W)
- R_{cb} = ballistic constriction resistance (K/W)
- R_{cd} = diffusive constriction resistance (K/W)
- R_{sub} = substrate thermal resistance (K/W)
- R_{tot} = total thermal resistance (K/W)
- $R_{\text{tot},d}$ = total diffusive thermal resistance (K/W)
- R_{wire} = wire thermal resistance (K/W)
- T = temperature field (K)
- T_{slip} = slip temperature of gas molecules (K)
- T_{wall} = wall temperature at gas-solid interface (K)
- ΔT_{jump} = temperature drop across the constriction (K)
- ΔT_{sub} = temperature drop in the substrate (K)
- ΔT_{sphere} = temperature drop in the sphere (K)
- ΔT_{wire} = temperature drop in the wire (K)

Greek Symbols

- α_g = thermal accommodation coefficient of gas molecules
- γ = correction factor for resistance in the transition regime
- η = ratio of specific heats
- τ = relaxation time of phonons (s)
- θ = dimensionless temperature profile
- μ = dynamic viscosity of gas ($\text{kgm}^{-1} \text{s}^{-1}$)
- ρ = density of gas molecules (kgm^{-3})
- ω = phonon frequency (rads^{-1})
- $d\Omega$ = incremental solid angle (sr)

References

- [1] Cahill, D. G., Ford, W. K., Goodson, K. E., Mahan, G. D., Majumdar, A., Maris, H. J., Merlin, R., and Phillpot, S. R., 2003, "Nanoscale Thermal Transport," *J. Appl. Phys.*, **93**(2), pp. 793–818.
- [2] Huxtable, S. T., Cahill, D. G., Shenogin, S., Xue, L., Ozisik, R., Barone, P., Usrey, M., Strano, M. S., Siddons, G., Shim, M., and Koblinski, P., 2003, "Interfacial Heat Flow in Carbon Nanotube Suspensions," *Nature Mater.*, **2**(11), pp. 731–734.
- [3] Kumar, S., Murthy, J. Y., and Alam, M. A., 2005, "Percolating Conduction in Finite Nanotube Networks," *Phys. Rev. Lett.*, **95**(6), p. 066802.
- [4] Yang, R., and Chen, G., 2004, "Thermal Conductivity Modeling of Periodic Two-Dimensional Nanocomposites," *Phys. Rev. B*, **69**(19), p. 195316.
- [5] Martel, R., Schmidt, T., Shea, H. R., Hertel, T., and Avouris, Ph., 1998, "Single- and Multi-Wall Carbon Nanotube Field-Effect Transistors," *Appl. Phys. Lett.*, **73**(17), pp. 2447–2449.
- [6] Xiang, J., Lu, W., Hu, Y., Wu, Y., Yan, H., and Lieber, C. M., 2006, "Ge/Si Nanowire Heterostructures as High-Performance Field-Effect Transistors," *Nature (London)*, **441**, pp. 489–493.
- [7] Pop, E., Mann, D., Goodson, K. E., and Dai, H., 2007, "Electrical and Thermal Transport in Metallic Single-Wall Carbon Nanotubes on Insulating Substrates," *J. Appl. Phys.*, **101**(9), p. 093710.
- [8] Pop, E., 2008, "The Role of Electrical and Thermal Contact Resistance for Joule Breakdown of Single-Wall Carbon Nanotubes," *Nanotechnology*, **19**(29), p. 295202.
- [9] Mingo, N., and Broido, D. A., 2005, "Carbon Nanotube Ballistic Thermal Conductance and Its Limits Export," *Phys. Rev. Lett.*, **95**(9), p. 096105.
- [10] Cola, B. A., Xu, X., and Fisher, T. S., 2007, "Increased Real Contact in Thermal Interfaces: A Carbon Nanotube/Foil Material," *Appl. Phys. Lett.*, **90**(9), p. 093513.
- [11] Cola, B. A., Xu, J., Cheng, C., Hu, H., Xu, X., and Fisher, T. S., 2007, "Photoacoustic Characterization of Carbon Nanotube Array Thermal Interfaces," *J. Appl. Phys.*, **101**(5), p. 054313.
- [12] Linderman, R., Brunschweiler, T., Smith, B., and Michel, B., 2007, "High-

Performance Thermal Interface Technology Overview," THERMINIC, Budapest, Hungary.

- [13] Shi, L., and Majumdar, A., 2002, "Thermal Transport Mechanisms at Nanoscale Point Contacts," *ASME J. Heat Transfer*, **124**, pp. 329–337.
- [14] King, W. P., and Goodson, K. E., 2002, "Thermal Writing and Nanoimaging With a Heated Atomic Force Microscope Cantilever," *ASME J. Heat Transfer*, **124**, p. 597.
- [15] Prasher, R., 2005, "Predicting the Thermal Resistance of Nanosized Constrictions," *Nano Lett.*, **5**(11), pp. 2155–2159.
- [16] Bahadur, V., Xu, J., Liu, Y., and Fisher, T. S., 2005, "Thermal Resistance of Nanowire-Plane Interfaces," *ASME J. Heat Transfer*, **127**(6), pp. 164–168.
- [17] Duan, X., Niu, C., Sahi, V., Chen, J., Parce, J., Parce, J. W., Empedocles, S., and Goldman, J. L., 2003, "High-Performance Thin-Film Transistors Using Semiconductor Nanowires and Nanoribbons," *Nature (London)*, **425**, pp. 274–278.
- [18] Lifshitz, R., and Roukes, M. L., 2000, "Thermoelastic Damping in Micro- and Nanomechanical Systems," *Phys. Rev. B*, **61**(8), pp. 5600–5609.
- [19] Bernasconi, A., Sleator, T., Posselt, D., Kjems, J. K., and Ott, H. R., 1992, "Dynamic Properties of Silica Aerogels as Deduced From Specific-Heat and Thermal-Conductivity Measurements," *Phys. Rev. B*, **45**, pp. 10363–10376.
- [20] Domingues, G., Rochais, D., and Volz, S., 2008, "Thermal Contact Resistance Between Two Nanoparticles," *J. Comput. Theor. Nanosci.*, **5**(2), pp. 153–156.
- [21] Prasher, R., 2006, "Ultralow Thermal Conductivity of a Packed Bed of Crystalline Nanoparticles: A Theoretical Study," *Phys. Rev. B*, **74**, p. 165413.
- [22] Zhang, J., Fisher, T. S., Ramachandran, P. V., Gore, J. P., and Mudawar, I., 2005, "A Review of Heat Transfer Issues in Hydrogen Storage Technologies," *ASME J. Heat Transfer*, **127**, pp. 1391–1399.
- [23] Wexler, G., 1966, "The Size Effect and the Non-Local Boltzmann Transport Equation in Orifice and Disk Geometry," *Proc. Phys. Soc. London*, **89**, pp. 927–941.
- [24] Sharvin, Y. V., 1965, "A Possible Method for Studying Fermi Surfaces," *Sov. Phys. JETP*, **21**, pp. 655–656.
- [25] Nikolić, B., and Allen, P. B., 1999, "Electron Transport Through a Circular Constriction," *Phys. Rev. B*, **60**(6), pp. 3963–3969.
- [26] McGee, G. R., Schankula, M. H., and Yovanovich, M. M., 1985, "Thermal Resistance of Cylinder-Flat Contacts: Theoretical Analysis and Experimental Verification of a Line-Contact Model," *Nucl. Eng. Des.*, **86**, pp. 369–381.
- [27] Yovanovich, M. M., 1967, "Thermal Contact Resistance Across Elastically Deformed Spheres," *J. Spacecr. Rockets*, **4**(1), pp. 119–122.
- [28] de Jong, M. J. M., 1994, "Transition From Sharvin to Drude Resistance in High Mobility Wires," *Phys. Rev. B*, **49**(11), pp. 7778–7781.
- [29] Sondheimer, E. H., 1952, "The Mean Free Path of Electrons in Metals," *Adv. Phys.*, **1**(1), pp. 1–42.
- [30] Pascual-Gutiérrez, J. A., Murthy, J. Y., and Viskanta, R. V., 2007, "Limits of Size Confinement in Silicon Thin Films and Wires," *J. Appl. Phys.*, **102**(3), p. 034315.
- [31] Schwab, K., Henriksen, E. A., Worlock, J. M., and Roukes, M. L., 2000, "Measurement of the Quantum of Thermal Conductance," *Nature (London)*, **404**, pp. 974–977.
- [32] Cross, M. C., and Lifshitz, R., 2001, "Elastic Wave Transmission at an Abrupt Junction in a Thin Plate With Application to Heat Transport and Vibrations in Mesoscopic Systems," *Phys. Rev. B*, **64**(8), p. 085324.
- [33] Prasher, R., Tong, T., and Majumdar, A., 2007, "An Acoustic and Dimensional Mismatch Model for Thermal Boundary Conductance Between a Vertical Mesoscopic Nanowire/Nanotube and a Bulk Substrate," *J. Appl. Phys.*, **102**(10), p. 104312.
- [34] Saha, S., and Shi, L., 2007, "Molecular Dynamics Simulation of Thermal Transport at a Nanometer Scale Constriction in Silicon," *J. Appl. Phys.*, **101**, p. 074304.
- [35] Chung, J. D., and Kaviani, M., 2000, "Effects of Phonon Pore Scattering and Pore Randomness on Effective Conductivity of Porous Silicon," *Int. J. Heat Mass Transfer*, **43**(4), pp. 521–538.
- [36] Murthy, J. Y., Narumanchi, S. V. J., Pascual-Gutiérrez, J. A., Wang, T., Ni, C., and Mathur, S. R., 2005, "Review of Multiscale Simulation in Submicron Heat Transfer," *Int. J. Multiscale Comp. Eng.*, **3**(1), pp. 5–32.
- [37] Murthy, J. Y., and Mathur, S. R., 2002, "Computation of Sub-Micron Thermal Transport Using an Unstructured Finite Volume Method," *ASME J. Heat Transfer*, **124**(6), pp. 1176–1181.
- [38] Chen, G., 1998, "Thermal Conductivity and Ballistic Phonon Transport in the Cross-Plane Direction of Superlattices," *Phys. Rev. B*, **57**(23), pp. 14958–14973.
- [39] Vincenti, W. J., and Kruger, C. H., 1965, *Introduction to Physical Gas Dynamics*, Wiley, New York.
- [40] Gad-el-Hak, M., 2001, *The MEMS Handbook*, 1st ed., CRC, Boca Raton, FL.
- [41] Wadsworth, D. C., 1993, "Slip Effects in a Confined Rarefied Gas. I: Temperature Slip," *Phys. Fluids A*, **5**(7), pp. 1831–1839.
- [42] Singh, D., Guo, X., Alexeenko, A., Murthy, J. Y., and Fisher, T. S., 2009, "Modeling of Subcontinuum Thermal Transport Across Semiconductor-Gas Interfaces," *J. Appl. Phys.*, **106**, p. 024314.
- [43] Fu, C. J., and Zhang, Z. M., 2006, "Nanoscale Radiation Heat Transfer for Silicon at Different Doping Levels," *Int. J. Heat Mass Transfer*, **49**, pp. 1703–1718.